Journal of Hydroscience and Hydraulic Engineering
Vol. 30, No.1 May, 2012, 87-99

ANALYSIS OF HYDRAULIC AND GEOMORPHIC CONDITIONS CAUSING RAILWAY EMBANKMENT BREACH DUE TO INUNDATION FLOW

By

Ryota Tsubaki

Department of Civil and Environmental Engineering, Hiroshima University, Higashi-hiroshima, Hiroshima, Japan

Yoshihisa Kawahara

Department of Civil and Environmental Engineering, Hiroshima University, Higashi-hiroshima, Hiroshima, Japan

Takahiro Sayama

International Center for Water Hazard and Risk Management, Public Works Research Institute, Minamihara, Tsukuba, Japan

and

Ichiro Fujita

Department of Civil Engineering, Kobe University, Rokkodai, Nada, Kobe, Japan

SYNOPSIS

Embankments on a floodplain, usually treated as solid walls in inundation simulations can cause considerable damage during severe flood events. The damage to road or railway embankment system not only changes the propagation of inundation flow but also destroys the transportation infrastructure. In this study, the failure of the embankment system of the Kishin Railway Line during the flood event in August, 2009 is analyzed. The factors in causing embankment failure are analyzed from the geographic and hydraulic view points. A framework to estimate the risk of the embankment failure, which is based on the analysis of the structures of the geography and inundation flow, is proposed in this work.

INTRODUCTION

The typhoon knows as Etau struck Japan in August 2009 with record-breaking heavy rainfall in Chugoku, Kansai, and Shikoku districts. The daily precipitation at Sayo-cho (Sayo Town) in Hyogo Prefecture reached much as 327 mm, which far exceeded the past record of 187 mm (Damage inspection committee of typhoon Etau of JSCE (1)). The heavy rainfall caused severe flooding in the catchment of the Chikusa River, flowing in the western part of Hyogo Prefecture, and also caused extensive damage including human casualties (Damage inspection committee of typhoon

Etau of Sayo-cho (2)) and the destruction of hydraulic structures and soil structures together with slope failure at many locations (Damage inspection committee of typhoon Etau of JGS (3)). Railway networks, such as the Kishin Line of West Japan Railway Company and the rail line of Chizu Express Company were also badly damaged. The Kishin Line had embankment failure, e.g. Fig. 1a, at 78 locations and suffered profound damage due to the submergence of railway stations and tracks over 3.8 km, which needed around two months for the whole line to restart (Kaneko (4)).

Road or railway embankments in a floodplain severely affect the extent of flood inundation. Hence it has been a common practice to take into account of the existence of embankments in flood inundation analyses. However, the analyses have not taken into consideration the embankment failure although the embankment breach in floodplain frequently occurs (see Fig. 1b). The reason for this is that the failure mechanism has not been clarified. Damage to road or railway embankments may disrupt transportation networks, leading to the delay in evacuation, restoration and reconstruction. Inundation flows may drastically change with the failure of embankment whose function is to store flooded water and alter flow direction (Kawaike et al. (5), Akiyama et al. (6)).

Fujita and Suwa (7) classified the damage caused by levee breach into

1. submergence of properties,
2. damage due to sediment or high speed flow and
3. lifeline damage accompanied by the failure of road or railway embankment.

They also emphasized the importance of formulating an effective countermeasure based on the understanding of outbreak mechanism of the disaster. The Hokuriku Regional Development Bureau (8) conducted a survey of the failures of road and railway embankments, and summarized the effects of failure and characteristics of the damage caused by the floods in steep slope rivers in comparison to that by floods in mild slope rivers, then developed the methodology to draw a flood projection map against the flooding from a steep slope river.

Although the important role and the risk of failure of the embankment in the floodplain during flooding are understood in the areas where rivers and the neighboring landform have steep slopes, the conditions of embankment failure have not been clarified and thus no method of predicting failures has been developed. Due to the crucial influence of the embankment failure on the lifelines and the inundation flows, it is important to analyze the damage to embankment and to predict its failure for the proper evaluation of the inundation damage, and for selecting suitable evacuation routes and taking precautions to prevent the embankment failure. Thus, this study aims at clarifying the mechanism of railway embankment failure, which occurred at many locations when the typhoon Etau struck in 2009, by analyzing the geomorphological features and the propagation of the inundation flow.

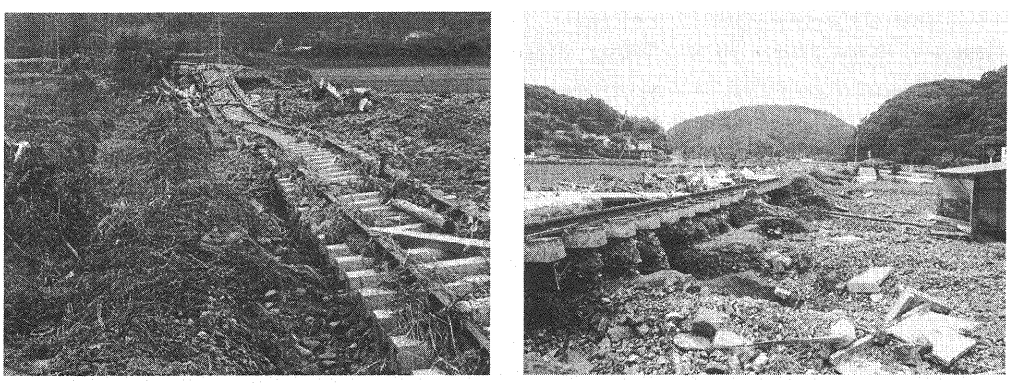

(a) August 2009, in Hyogo, Japan (b) July 2010, in Yamaguchi, Japan

Fig. 1 Damage to the embankments on a floodplain

DESCRIPTION OF THE DISASTER

In the present research, the causes of railway embankment damage as a result of inundated flood flow are investigated by conducting an inundation analysis with respect to the actual damage due to the typhoon Etau to the Kishin Line by the flooding of the Sayo River. The damaged points of the railway were concentrated in the area about 6 km upstream from the confluence with the Chikusa River. This section provides a general view of the rainfall distribution, topological features and embankment damage.

Rainfall features

The typhoon Etau broke out in the North Pacific on August 8 2009 and approached close to the Japanese mainland but moved towards the east without making landfall on Japan. It finally became a tropical cyclone five days later (Damage inspection committee of typhoon Etau of JSCE (1)). Although the magnitude of the typhoon itself was not so large, it brought a vast amount of moisture-laden air created on the Pacific Ocean to the Japan mainland, and this resulted in a record-breaking rainfall in the mountainous area in Tokushima, Kagawa, Okayama and Hyogo Prefectures. As an example, 24-hour rainfall distribution in the Chikusa River Basin in Hyogo Prefecture is shown in Fig.2. Obviously, the rainfall was concentrated mainly in the Sayo River Basin, where the 24-hour rainfall was more than 300 mm. This torrential rain was concentrated both in space and time, which resulted in the direct cause of flood disasters in the Sayo-cho area.

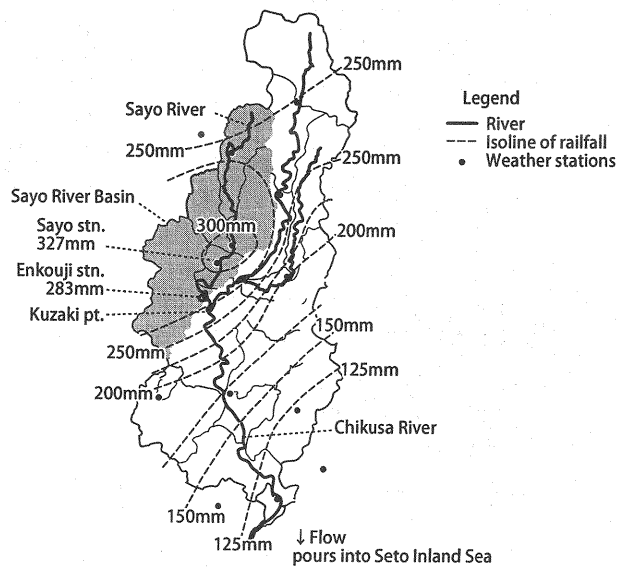

Fig. 2 Isolines of maximum 24-hour rainfall in the Chikusa River Basin. (Hyogo Prefecture (9))

Topological features

The Sayo River is a tributary of the Chikusa River, which is one of the class B rivers in Hyogo Prefecture, and merges into the main river at Kuzaki point (see Fig. 2). The Kishin Railway Line runs parallel to the Sayo River for about 6 km from about 6 kilopost (kp) to 12 kp measured from the confluence with the Chikusa River. The mean bed slope of the target reach varies between 1/220 and 1/310 and the river meanders in a narrow valley floor. Although the design highwater discharge of the Sayo River is 560 m^3/s (Hyogo Prefecture (10)), a number of river sections still have

insufficient discharge capacity due to the low ground level of backland, and deficiency in cross-sectional area and backwater ate affected by narrow sections. Since the river discharge induced by the typhoon Etau is estimated to be 800 m^3/s, far more than the design discharge, it resulted in inundations over most of the lower valley districts.

Damage to railway embankment

Damage to railway embankments caused by inundated flows occurred mainly along the area where the Sayo River and Kishin Line run parallel in the outskirt of Sayo-cho district, in which rainfall was extremely concentrated. Most of the damage occurred within the reach of about 13 km between Harimatokusa and Mimasaka-Doi Stations; the damages are ballast flushed away at 56 points, 13 slope failures and sediment influx and 9 severe breachings of embankment, etc. It should be noted that damage to ballasts and embankments took place to a greater degree between Sayo and Kozuki Stations since inundated flow directly hit railway lines in this area. Fig.3 shows locations of the railway damage as filled circles and the Sayo River and the Kishin Line. The numbers beside the filled circles indicate the kilopost of the Kishin Line. According to the field research (Kaneko (4)), the heaviest damage was observed at 49.2 kp, where an embankment about 2 m in height was washed away over 140 m and ballasts were damaged over 60 m beside the embankment breached area. As a result the railways became twisted and suspended because of the hydrodynamic forces due to the inundated flow as shown in Fig.1a.

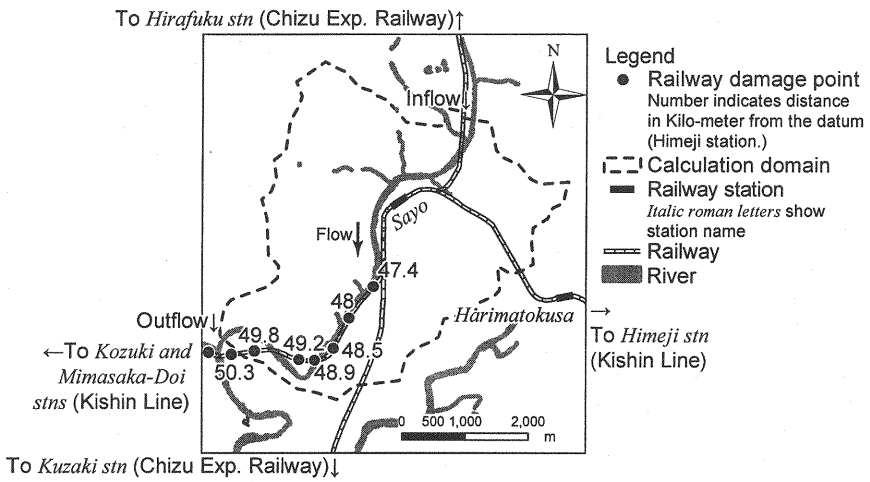

Fig. 3 Locations of railway embankment damage.

HYDROLOGICAL ANALYSIS

A rainfall-runoff simulation is conducted for the Sayo River Basin (190 km^2 in area: upstream of the Enkouji observation station). The main objectives of the simulation are to estimate boundary conditions for the inundation analysis to be conducted in the following section as well as to investigate the characteristics of rainfall-runoff processes during the Etau flood event. We used a 50 m resolution distributed model that simulates both rainfall-runoff processes from mountainous slopes and flood routing in river channels based on kinematic wave equations (Tachikawa et al. (11), Sayama et al. (12)). The equations applied to the mountainous slopes are the lateral components of unsaturated, saturated subsurface and surface flows by the equation (1) and the water mass balance equation (2).

$$q=\begin{cases} d_m k_m\left(\dfrac{h}{d_m}\right)^{\beta} i, & (0\le h\le d_m) \\ (h-d_m)k_a i + d_m k_m i, & (d_m < h\le d_a) \\ \dfrac{\sqrt{i}}{n}(h-d_a)^m + (h-d_m)k_a i + d_m k_m i & (d_a < h) \end{cases} \quad (1)$$

$$\frac{\partial h}{\partial t}+\frac{\partial q}{\partial x}=r(t) \quad (2)$$

where d_m and d_s denote the water depth corresponding to the water content in unsaturated zone and saturate zone respectively, k_a is the saturated hydraulic conductivity, k_m is the unsaturated hydraulic conductivity, β is the ratio between saturated and unsaturated hydraulic conductivities ($=k_a/k_m$), i is slope, n is the Manning's roughness coefficient, r is the rainfall intensity. The h and q denote water depth and discharge per unit width at time t and location x. Input data used for this simulation was radar-gauge composite data.

Fig. 4 shows the simulated and observed hydrographs at the Enkouji observation station. The observed discharge hydrograph was estimated based on the recorded water stage hydrograph and the rating curve. The calibrated parameters were n = 0.3 s/m$^{1.3}$, k_a = 0.015 m/s, d_a = 0.4 m, d_m = 0.0 m, which implies that only the saturated subsurface and surface flows were sufficient to reproduce the observed hydrograph at Enkouji without incorporating the unsaturated subsurface flow that is often important for representing soil water storing in the catchment. The calculated runoff ratio in this simulation was 0.85, which corresponds to the small amount of catchment storage during the flood event. Since the model used here is a distributed type, the calibrated model can be now used to estimate hydrographs in small tributaries. Fig. 5 shows the hydrographs estimated at the tributary depicted in Fig. 3 that are used as the boundary conditions and source term for inundation analysis which is explained in the next section.

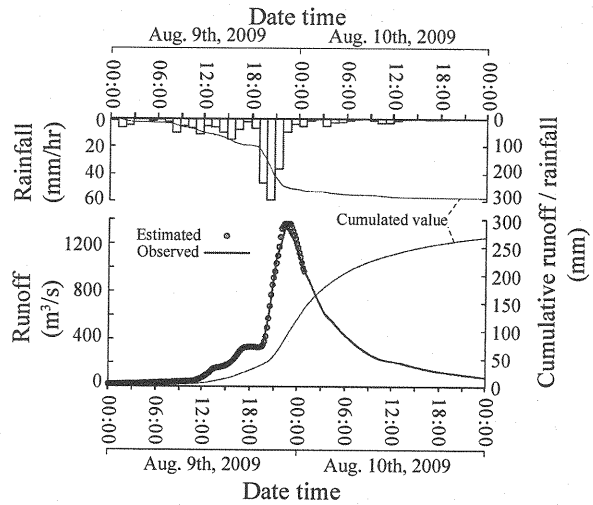

Fig. 4 Simulated and observed hydrographs at Enkouji station. Note that the observed discharge is missing from 1:00 August 10. The simulation period is from 0:00 August 9 (= 0h) to 0:00 August 11 (=48h) in 2009.

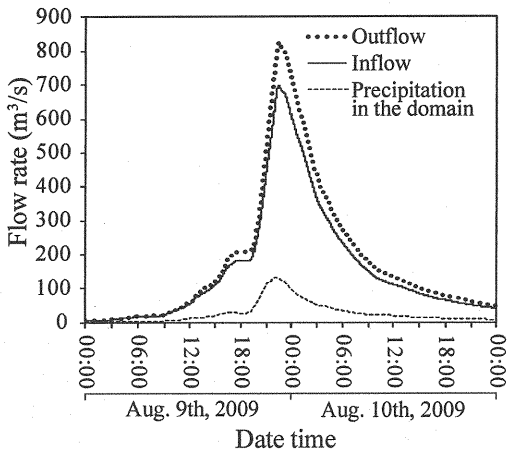

Fig. 5 Estimated inflow, outflow and rainfall hydrographs of the domain used in inundation flow simulation. Precipitation in the domain stands for the total rain fall in the domain per unit time.

INUNDATION FLOW SIMULATION

The river and inundation flows were calculated by solving the shallow water equations (Tsubaki and Fujita (13)). The scalar transport equation was also solved (Benkhaldoun et al. (14)) to discriminate the source (overflow from river or precipitation) of the inundated water. The basic equations solved here are as follows:

$$\frac{\partial U}{\partial t}+\frac{\partial E}{\partial x}+\frac{\partial F}{\partial y}=S \tag{3}$$

$$\begin{aligned} U &= \left(h \quad hu \quad hv \quad hc\right)^T, \\ E &= \left(hu \quad hu^2+0.5gh^2 \quad huv \quad huc\right)^T, \\ F &= \left(hv \quad huv \quad hu^2+0.5gh^2 \quad hvc\right)^T, \\ S &= \left(q_s \quad gh\left(S_{0x}-S_{fx}-S_{Hx}\right) \quad gh\left(S_{0y}-S_{fy}-S_{Hy}\right) \quad 0\right)^T. \end{aligned} \tag{4}$$

where t is the time, x and y are the horizontal coordinates, h is the water depth, u and v are the depth-averaged velocities in the x- and y- directions, c is the scalar density, g is the gravitational acceleration, q_s is the source in water mass due to rain fall, S_{0x} and S_{0y} are the bed slopes in the x- and y- directions and calculated using the ground elevation z as

$$S_{0x}=-\frac{\partial z}{\partial x},\ S_{0y}=-\frac{\partial z}{\partial y}. \tag{5}$$

S_{fx} and S_{fy} are the friction slopes evaluated by using the Manning's roughness coefficient n as follows.

$$S_{fx}=\frac{n^2u\sqrt{u^2+v^2}}{h^{4/3}},\ S_{fy}=\frac{n^2v\sqrt{u^2+v^2}}{h^{4/3}}. \tag{6}$$

S_{Hx} and S_{Hy} are the energy slope due to the bridge with piers. These terms are effective only at the cell interface located

in the bridge cross-section.

$$S_{Hx} = -\frac{\partial H_b}{\partial x}, S_{Hy} = -\frac{\partial H_b}{\partial y} \tag{7}$$

where H_b is the head loss due to the bridge. The amount of head loss is calculated by using D'Aubuisson's empirical formula (Chow (15), Sakano, (16)), namely

$$\Delta h = \frac{Q^2}{2g}\left(\frac{1}{c_c^{\,2} b_2^{\,2}(h_1 - \Delta h)^2} - \frac{1}{b_1^{\,2} h_1^{\,2}}\right). \tag{8}$$

Here, Δh is the afflux due to the bridge, Q is the flow rate through the cross-section, c_c is a parameter related to the flow separation around the obstacle and c_c=1.0 is used after the calibration by Sakano (15), b is the effective width of flow and subscript 1 and 2 correspond to the upstream and downstream of the bridge cross section, repsectively, h_1 is the water depth upstream of the bridge section. The flow parameters related to the bridge head loss are shown in Fig. 6. Q in equation (8) is calculated as $Q=\boldsymbol{U}_1 \cdot \boldsymbol{n}$, where $\boldsymbol{U}_1$ is the approaching velocity vector and $\boldsymbol{n}$ is the normal vector of the cross-section. b_2 denotes the effective width which represents the cross-sectional area deficit by the bridge structure. To correlate Δh and slope of H_b, Bernoulli's equation is used, namely

$$\frac{\left(\overline{h_2} + \frac{1}{2\overline{h_2}^{\,2}}\right) - \left(\overline{h_1} + \frac{1}{2\overline{h_1}^{\,2}}\right)}{h_c} = H_b, \tag{9}$$

where $\overline{h_1}$ and $\overline{h_2}$ are the water depth normalized by the critical water depth, which is calculated as

$$h_c = \sqrt[3]{\frac{|U|^2 h^2}{g}}. \tag{10}$$

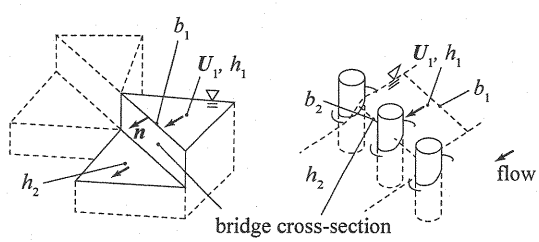

(a) Discritized (b) Actual

Fig. 6 Distribution of flow parameter concerning about bride head loss.

The equations were solved by means of the finite volume method using the unstructured triangulate grid system. The flux difference scheme (FDS) was used to evaluate fluxes through the boundary of the triangular cell. The Euler explicit method was used for time marching. The domain represented in the inundation simulation was about 15 km^2 in area. The calculation grid representing the domain is shown in Fig. 7. In this area, the Sayo River flows, and there are

no major tributaries converging to the Sayo River. The elevation data for the calculation grid was configured using aerial LiDAR (Light Detection and Ranging) for the riverside region, and the 50-m grid DEM (Digital Elevation Model) was utilized for the intermountain area. A comparatively small grid size (3 m for the length of a side of a triangle) was used around the river and the railway to represent the details of the topography (Bates et al. (17), Cobby (18), Rath and Bajat (19)). In the mountain area, a larger grid size (40 m in length) was used to save the computational load. Manning's roughness parameter n was set to 0.02 for the river bed and the plain land, 0.1 for the vegetation in the river course and the inundated area and the residential area, and 0.3 for the mountainous area. For inflow boundary condition, the discharge hydrograph depicted in Fig. 5 was used. The rating curve at the outflow cross-section was estimated and the flow rate at the outflow cross-section calculated by the hydrological model was converted to the water stage. The source term in the mass conservation (q_s in Equation (4)) represents the precipitation in this area and the runoff ratio 0.85 was multiplied for gross precipitation.

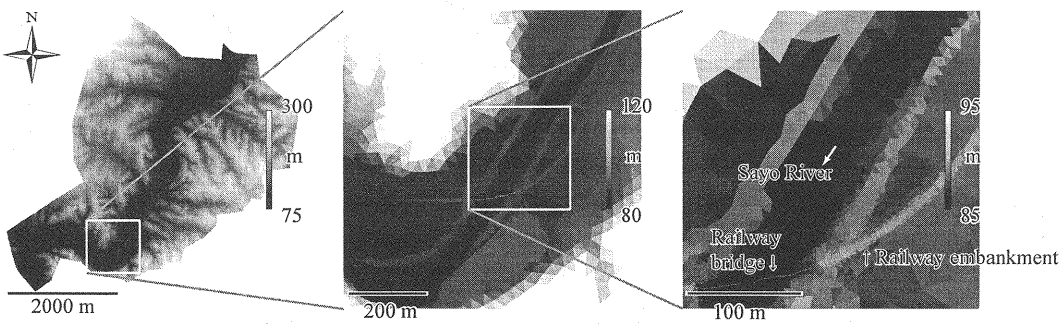

Fig. 7 Calculation grid of simulated tributary. The gray-scale shading corresponds to the elevation.

VALIDATION OF INUNDATION FLOW SIMULATION

To validate the inundation flow model, the calculated results are compared with the inundation records. As shown in Fig. 8, the calculated inundated area almost corresponds to the record of the inundation area. In Fig. 9, the local water stage and the water depth of calculated and recorded inundated water stages and water depths are compared. The calculated water stage stands for $h + z$ in the basic equations. The mean absolute error is 0.28 m, and the magnitude of the error is smaller than, but comparable to, the magnitude of inundated water depth, 1 m. The discrepancy between the calculated and recorded water stages may be related to the error of LiDAR data used in the topography data used for the calculation. Moreover, there is a difference in the definitions of calculated and recorded water depths, namely the calculated water depth is a cell averaged quantity but the recorded water depth denotes the local water depth around obstacles and this caused an under estimation in the calculated water depth shown in the right side of Figure 9.

In conclusion, in the validation, the calculated results generally represents the main feature of the inundation. On the contrary, we observed that there was considerable uncertainty in the calculated result. This uncertainty is related to not only the model used to represent the inundation but also the recorded water stage and topographical information. In this context, to analyze the local flow, it is necessary to keep in mind that the calculated result contains comparatively large uncertainties.

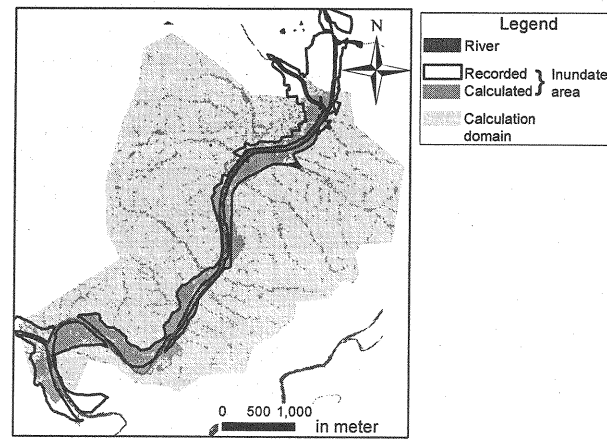

Fig. 8 Comparison of calculated and recorded inundated areas.

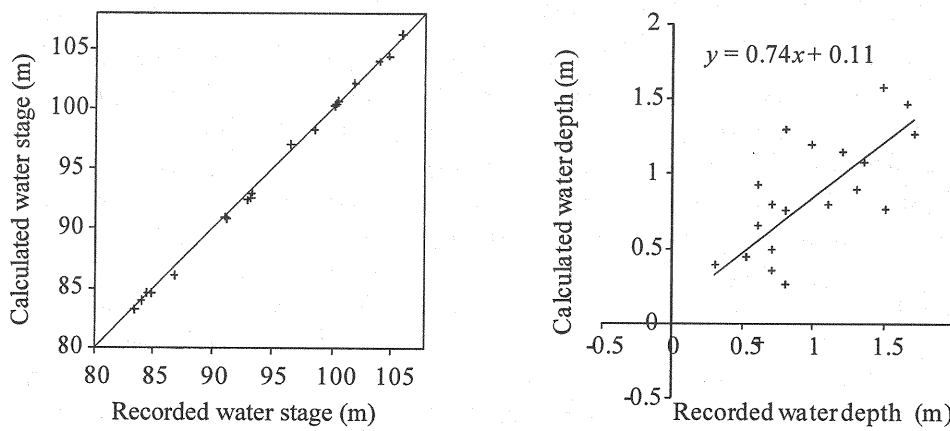

Fig. 9 Comparison of calculated and recorded inundated water stages and water depths.

DAMAGE TO RAILWAY EMBANKMENT

To understand the fundamental relationship between the railway embankment damage and topography, longitudinal elevation profiles of the railway embankment and the river bank are compared in Fig. 10. The elevation shown here was based on the LiDAR data which has an elevation accuracy of 0.15 m. As shown in the figure, the elevation of railway embankment is similar in profile to the river bank elevation. The ballast loss due to the overflow, depicted as open circles, was observed in the regions where the railway embankment shows a comparatively mild and constant slope. On the other hand, the location of the embankment breach damage, shown as filled diamond symbols in Figure 10, corresponds to the convex downward large curvature region of the railway embankment. In the area of mild and constant slope embankment, the flood water overflowed over a relatively large segment with a low overflow water depth. However, in the convex downward segment, the overflow of the inundated water was concentrated in the bottom of the convex, which made the overflow water depth comparatively large. This concentration of overflow caused the embankment breach.

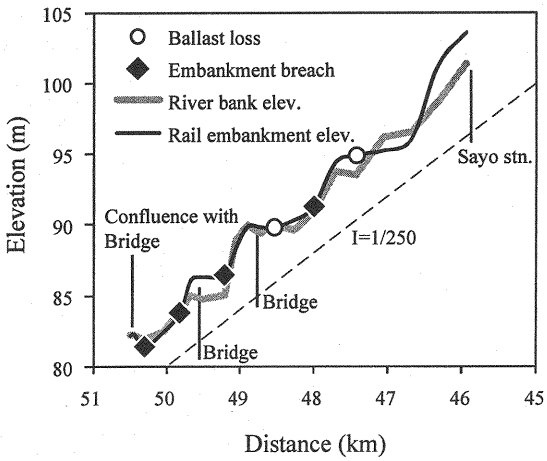

Fig. 10 Longitudinal elevation profiles of the railway and the riverbank. The cross-sections where the river and railway intersects are indicated as the 'bridge'.

Fig. 11 depicts the structure of inundation flow at the moment around the peak inundation period is depicted. The flow structure is visualized using the Line Integral Convolution (LIC) technique (Cabral and Leedom (20)). Here, the direction of texture corresponds to the local flow direction, and the density of the texture correlates with the local flow discharge per unit width. The dense (darker) meandering path in Fig. 11 corresponds to the river course. The light gray (lighter) path-lines surrounding the river course indicate the course of the inundated water that flowed on the flood plain. The numbered circles and diamond symbols in the bottom figure in Fig.11 depict the location of the railway damage. The points where railway embankment was damaged correspond to the area where the inundation water flowed in a concentrated manner. This local flow concentration is regulated by a topographical structure, namely the slope of the surrounding mountains. The points labeled with 47.4, 48 and 48.5 are located in the boundary of the inundation flow, and these points correspond to the areas where comparatively little damage was observed. The point 49.8 is isolated from the inundation flow. In this area, ballast loss was observed after the rainfall event, and such damage was due to not the overflow water from the river course but the direct runoff from the adjacent mountain slope. At 49.2 and 50.3 points, the inundated flow completely enclosed to these damaged segments. The consecutive and comprehensive flow of inundation around the railway path is a crucial factor in causing severe breaching of the railway embankment at 49.2 and 50.3 points. The damage at 48.9 was due to the river bank erosion, so there is no direct relation between the damage and inundation flow at this point because river bank erosion was not modeled in the calculation. There is no clear relation between the intensity of the railway damage and the horizontal inundation flow structure. Analyzing both longitudinal and horizontal structures of topography and inundation flow should be useful in evaluating the risk of the railway damage due to the inundation.

The structure of the inundation flow is determined by the structure of geographical features and the boundary flow conditions, and is not particularly sensitive to the uncertainty of a local flow and small differences in boundary conditions. Therefore, to predict the damage risk robustly and effectively, it is very important to pay attention to the structure of inundation flow and its relation to geomorphic conditions.

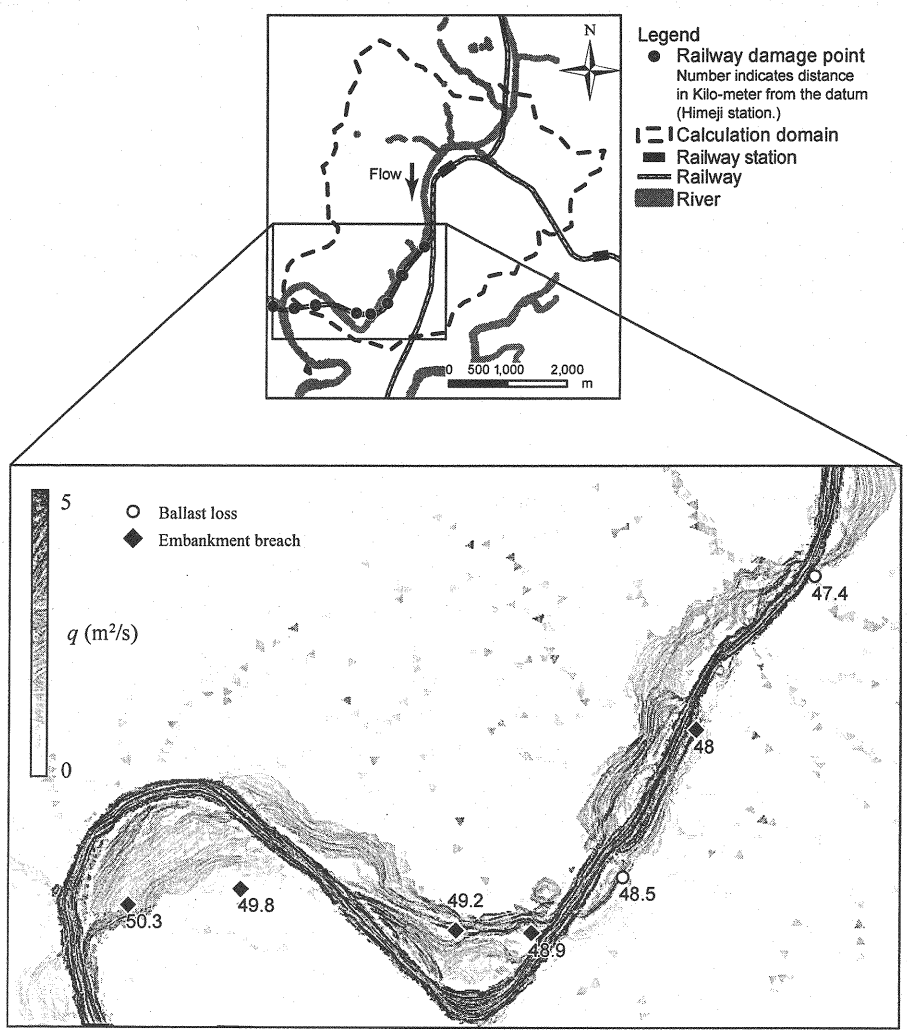

Fig. 11 Flow structure visualization using LIC technique. The direction of texture corresponds to the flow direction. The density of texture represents the magnitude of flow (unit discharge q).

CONCLUSION

In this study, damage to the embankment of the Kishin Line during the flood event in August 2009 was analyzed. The topographic and hydraulic conditions were correlated with the embankment failure. The essential structure of the inundation flow was represented by using the LIC technique. Understanding and analyzing the structure of inundation flows and their relation to the topography are essential for estimating the potential of the embankment failure and the damage related to inundation flows.

It was clarified that simulated local flow condition retained a considerable degree of uncertainty. Due to the difficulty of predicting flow precisely, we should assume that estimation of damage based on the local flow conditions, such as the local water depth or velocity, also exhibits a large degree of uncertainty. The damage prediction based on

not local flow condition but the coherent structure of the inundation (Tsubaki et al. (21)) is a promising area to be researched strenuously. The modern flow visualization technique, e.g. LIC, is a useful and an essential tool for analyzing the structure of the inundation flows and for predicting the damage related to the flow of inundations.

ACKNOWLEDGMENTS

This work was partially funded by grants from the Chugoku Civil Engineering Foundation for Mutual Aid, Japan and the Foundation for River and Watershed Environment Management, Japan. The first author acknowledges Dr. Ichiro Ario at Hiroshima University for his useful suggestions at the start of the study.

REFERENCES

1. Damage inspection committee of typhoon Etau of JSCE (Japan society of civil engineers): Technical report on the damage due to the typhoon Etau, JSCE, 2010 (in Japanese).
2. Damage inspection committee of typhoon Etau of Sayo-cho: Report on damage due to typhoon Etau, Sayo-cho, 2010 (in Japanese).
3. Damage inspection committee of typhoon Etau of JGS (Japan Geotechnical Society): Report on damage in geotechnical structures due to typhoon Etau, 2009 (in Japanese).
4. Kaneko, Y.:, The damage to the railway of the Kishin Line between Kyutoku station to Mimasaka-doi station due to the typhoon Etau, J. of Japan Rail Way Civil Eng. Association, Vol.6, pp.450-451, 2010 (in Japanese).
5. Kawaike, K., Inoue, K., Toda, K. and Noguchim M.: Inundation flow analysis due to heavy rainfall in low-lying urbanized river basin, Journal of Japan Society of Civil Engineers, No.761/II-67, pp.57-68, 2004 (in Japanese).
6. Akiyama, J., Shige-eda, M., Tsuzaki, S. and Shigeoka, H.: Simulations of urban inundation and drainage processes in a hilly urban area, Annual Journal of Hydraulic Engineering, JSCE, Vol.51, pp.511-516, 2007 (in Japanese).
7. Fujita, K. and Suwa, Y.: Levee engineering necessary in the evolution from flood-disaster frequency reduction into its overall control, Advances in River Engineering, Vol.6, pp.1-6, 2000 (in Japanese).
8. Saito, J., Shirai, M., Wakigawa, K., Kanazawa, H. and Sako, S.: A study on flood hazard areas based on the characteristics of flooding from steep slope river, Advances in River Engineering, Vol.9, pp.143-148, 2003 (in Japanese)
9. Hyogo Prefecture: Inundated area due to the typhoon Etau, 2010 (in Japanese).
10. Hyogo Prefecture: River management plan for Sayo River, 2005 (in Japanese).
11. Tachikawa , R., Shrestha, R. and Sayama, T.: Flood prediction in Japan and the need for guidelines for flood runoff modelling in predictions in ungauged basins, International Perspectives on the State of the Art and Pathways Forward, IAHS Publ. 301, pp. 78-86, 2006
12. Sayama, K., Kobayashi, K. and Takara, K.: The hydrological analysis of the flood due to the typhoon Etau, in Technical report on the damage due to the typhoon Etau, JSCE, 2010 (in Japanese).
13. Tsubaki, R., Fujita, I.: Unstructured grid generation using LiDAR data for urban flood inundation modelling, Hydrological Processes, Vol.24, pp.1404-1420, 2010.
14. Benkhaldoun, F. et al.: Well-balanced finite volume schemes for pollutant transport by shallow water equations on unstructured meshes, J. of Comp. Phys., Vol.226, pp. 180-203, 2007.
15. Chow, V.T.: Open-channel hydraulics, McGraw Hill Book Company, 1959 (reprinted by Blackburn Press).
16. Sakano, A.: Hydraulic study on accumulation of drifting wood at a bridge during a flood, Technical note of National Institute for Land and Infrastructure Management, No.78, 2003 (in Japanese).

17. Bates, P.D., Marks, K.J., Horritt, M.S.: Optimal use of high-resolution topographic data in flood inundation models, Hydrological processes, Vol.17, pp.537-557, 2003.
18. Cobby, D.M. et al. Mason, D.C., Horritt, M.S., Bates, P.D.: Two-dimensional hydraulic flood modeling using a finite-element mesh decomposed according to vegetation and topographic features derived from airborne scanning laser altimetry, Hydrological processes, Vol.17, pp.1979-2000, 2003.
19. Rath, S., Bajat, B.: Between sensing, Forecasting and risk assessment: an integrated method to model high resolution data for floodplain representations in hydrodynamic simulations, Proceedings of the 1st Goettingen Remote Sensing Days, Goettingen, 2004.
20. Cabral, B. and Leedom, L.: Imaging vector fields using line integral convolution, Proc. 20th annual conf. on Computer graphics and interactive techniques SIGGRAPH 93, 1993.
21. Tsubaki, R., Fujita, I., Okabe, T.: Sensitivity of grid spacing to prediction and coherent flow structure of inundation on urbanized area, 32nd congress of IAHR, Venice, 2007.

APPENDIX – NOTATION

The following symbols are used in this paper:

b_1, b_2 = approaching and reduced widths of bridge cross-section [m];
c = passive scaler transported with flow [-];
c_c = correction factor for effective width of flow [-];
d = distance between neighboring cell centers [m];
d_m = water depth corresponding to the water content in unsaturated zone [m];
g = gravity acceleration;
h = water depth [m];
i = slope [-];
k_a = saturated hydraulic conductivity [m/s];
k_m = unsaturated hydraulic conductivity [m/s];
n = Manning's roughness coefficient [s/m$^{1/3}$];
r = rainfall intensity [mm/hr];
q = discharge per unit width [m^2/s];
q_s = source in water mass representing precipitation [m/s];
S_{0x}, S_{0y} = bed slopes in x and y directions [-];
S_{fx}, S_{fy} = friction slopes in x and y directions [-];
S_{Hx}, S_{Hy} = energy slopes in x and y directions due to the head loss by the bridge pier [-];
t = time [s];
u, v = depth averaged velocity components correspond to x and y coordinates [m/s];
x, y = horizontal coordinates [m]; and
β = ratio between saturated and unsaturated hydraulic conductivities ($=k_a/k_m$) [-].

(Received Aug, 01, 2011 ; revised Apr, 02, 2012)